

## Draping of biaxial non-crimp fabric on hemispherical shape

ZHENG Ruochen<sup>1</sup>, NAOUAR Naim<sup>1,a\*</sup>, SCHÄFER Bastian<sup>2</sup>, PLATZER Auriane<sup>1</sup>,  
COLMARS Julien<sup>1</sup>, KÄRGER Luise<sup>2</sup>, BOISSE Philippe<sup>1</sup>

<sup>1</sup>Univ Lyon, INSA-Lyon, CNRS UMR5259, LaMCoS, F-69621, France

<sup>2</sup>Karlsruhe Institute of Technology (KIT), Institute of Vehicle System Technology (FAST),  
Karlsruhe, Germany

<sup>a</sup>naim.naouar@insa-lyon.fr

**Keywords:** Biaxial NCF, Hyperelastic, Meso-Scale Model, Composite Forming

**Abstract.** The experiment and simulation of biaxial non-crimp fabric draping process is investigated. The finite element model is formulated employing a mesoscopic approach, wherein each individual fiber yarn and stitch is treated as a continuous medium, modeled separately for a more nuanced representation. The hemispherical punch shape for the draping is selected as it is the most commonly used academic shape with a rather simple double-curved geometry. The deformed shape, material draw-in and local shear angle between the experimental and numerical results are compared and discussed.

### Introduction

Non-crimp-fabric (NCF) composite reinforcements are one of the most promising types of reinforcements for the manufacturing of composite parts in both the automotive and aeronautical industries [1,2,3]. They consist of multiple layers of unidirectional plies bound together by stitches that pass through their thickness. Fibers in NCFs are straight, without weakening undulations like in woven fabrics [4]. This type of reinforcement offers a significant advantage in achieving mechanical stiffness greater than that of a fabric with the same thickness.

The need for higher production rates and parts with better-controlled and optimized characteristics increase the difficulty of using NCFs for large-series production and give reasons for an improved virtual validation and process design. Their forming process involves shaping flat 2D fabric plies into complex 3D shapes using an external force through the punch [5]. Blank holders are generally used during this step to tension the fabric and delay the appearance of wrinkles [6]. A simulation code allows for numerical optimization of molds and reinforcements, thus avoiding a costly trial-and-error phase during the design of composite parts [7].

Significant research efforts are devoted to the behavior of NCF and the simulation of its deformation. Its deformation mechanisms involved are specific and are studied in [8,10]. The through thickness compaction behavior of uni- and bidirectional NCF are investigated in [9]. Macroscopic approach is commonly used to simulate NCF forming process [11,12,13,14]. However, this approach may face challenges in identifying certain local defects, particularly gapping, where adjacent yarns separate, leaving an empty zone without fibers. Detection of these gapping defects is typically achieved through numerical analysis of the in-plane transverse strain for unidirectional NCF at the macroscale [13,14]. An alternative approach involves employing mesoscopic simulation approach, wherein each fiber yarn is considered as solid medium and the surrounded stitches are modelled by finite beam or bar elements [15,16,17].

A mesoscopic approach for biaxial NCF is introduced and validated using a unit cell model [17]. Subsequently, this approach is applied to larger sample sizes comprising multiple unit cells for forming simulations in this study. The selection of the hemispherical punch shape is based on its simplicity as a double-curved geometry with a smooth curvature, suitable for fabric draping.

Despite the simplicity, in-plane shear deformation and potential defects like gapping or wrinkles can still occur. The experimental and numerical simulation results of draping of biaxial NCF are subsequently compared and discussed.

### Materials

The material used in this study is a warp-knitted  $0^\circ/90^\circ$  carbon fiber biaxial NCF with polyester tricot stitches produced by Zoltek. The two layers are bound together during the production process with loop formation in the warp direction. The photographs of bi-axial NCF on both sides are shown in Fig. 1.



Fig. 1.  $0^\circ/90^\circ$  tricot-stitch biaxial non-crimp fabric architecture (a) warp fiber yarn view with a tricot stitch pattern (b) weft fiber yarn view with a chain stitch pattern

### Mesoscopic simulation approach

**Geometrical model.** At the mesoscopic scale, the geometric modeling of biaxial NCF involves the independent representation of stitches and fiber yarns. Prior studies have assumed various cross-sectional shapes for fiber yarns, such as circular, flat, elliptic, or biconvex [18, 19]. In this study, fiber yarns are initially modeled with oval cross-sections and assumed to be straight along the fiber orientation. Node positions are determined using a 3D elliptic cylinder equation in Matlab, accounting for mesh size, and eight nodes form a solid element. The nodes along a single loop of stitch are calculated using the equilibrium equation of the elliptical fiber yarn. Following the assembly of fiber yarns and stitches, a simulation of stitch shrinkage is conducted to tighten the initially loose structure and establish effective interaction between yarn systems. The mesoscopic geometrical model of biaxial NCF is presented in Figure 2a and b.



Fig. 2. Geometrical model of biaxial NCF (a) warp yarn view (b) weft yarn view

**Constitutive model.** The polyester stitch is modeled as a linear elastic material, its Young's modulus is characterized through tensioning one single stitch and its bending stiffness is determined using a cantilever bending test, a well-established method utilized in previous studies [20,21,22].

The constitutive law utilized for the carbon fiber yarn is a hyperelastic model developed by A. Charmetant [23]. The stresses are derived from a strain energy potential that describes the mechanical behaviour of a single carbon fibre yarn. This model accounts for four deformation modes based on the assumption that the fibre yarn is transversely isotropic: elongation along the

fiber direction, cross-sectional compaction, transverse shear (cross-sectional distortion), and longitudinal shear along the fiber direction.

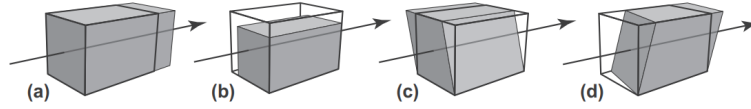


Fig. 3. Four deformation modes of fiber yarn (a) elongation (b) compaction of cross section (c) transverse shear (d) longitudinal shear

The hyperelastic equation defines the stress-strain relation for the solid by specifying its strain energy density  $w$  as a function of deformation gradient tensor:

$$w = w(\underline{\underline{F}}) \quad (1)$$

The four deformation modes are translated in the form of combinations of physical invariants,  $I_{\text{elong}}$ ,  $I_{\text{comp}}$ ,  $I_{\text{dist}}$ ,  $I_{\text{sh}}$ , linked to the invariants of the right Cauchy-Green tensor  $\underline{\underline{C}}$ .

These physically based invariants are introduced in [23] and are expressed as:

$$I_{\text{elong}} = \frac{1}{2} \ln I_4, \quad I_{\text{comp}} = \frac{1}{4} \ln \left( \frac{I_3}{I_4} \right), \quad I_{\text{dist}} = \frac{1}{2} \ln \left( \frac{I_1 I_4 - I_5}{2 \sqrt{I_3 I_4}} + \sqrt{\left( \frac{I_1 I_4 - I_5}{2 \sqrt{I_3 I_4}} \right)^2 - 1} \right), \quad I_{\text{sh}} = \sqrt{\frac{I_5}{I_4^2} - 1} \quad (2)$$

Where  $I_1$  to  $I_5$  are classical invariants expressed by the right Cauchy Green strain tensor  $\underline{\underline{C}}$ :

$$\begin{aligned} I_1 &= \text{trace}(\underline{\underline{C}}), \quad I_2 = \frac{1}{2} (\text{trace}(\underline{\underline{C}})^2 - \text{trace}(\underline{\underline{C}}^2)), \quad I_3 = \det(\underline{\underline{C}}), \\ I_4 &= \underline{\underline{C}} : \underline{\underline{M}}, \quad I_5 = \underline{\underline{C}}^2 : \underline{\underline{M}} \end{aligned} \quad (3)$$

Where  $\underline{\underline{M}}$  is a structural tensor defined by a unit vector of fiber direction  $\underline{\underline{M}}$ :

$$\underline{\underline{M}} = \underline{\underline{M}} \otimes \underline{\underline{M}} \quad (4)$$

Then the deformation energy is assumed to be the sum of the energies of these four deformation modes:

$$w(\underline{\underline{F}}) = w_{\text{elong}}(I_{\text{elong}}) + w_{\text{comp}}(I_{\text{comp}}) + w_{\text{dist}}(I_{\text{dist}}) + w_{\text{sh}}(I_{\text{sh}}) \quad (5)$$

The second Piola–Kirchhoff stress tensor is defined as:

$$\underline{\underline{S}} = 2 \frac{\partial w}{\partial \underline{\underline{C}}} = 2 \left( \frac{\partial w_{\text{elong}}}{\partial I_{\text{elong}}} \frac{\partial I_{\text{elong}}}{\partial \underline{\underline{C}}} + \frac{\partial w_{\text{comp}}}{\partial I_{\text{comp}}} \frac{\partial I_{\text{comp}}}{\partial \underline{\underline{C}}} + \frac{\partial w_{\text{dis}}}{\partial I_{\text{dis}}} \frac{\partial I_{\text{dis}}}{\partial \underline{\underline{C}}} + \frac{\partial w_{\text{sh}}}{\partial I_{\text{sh}}} \frac{\partial I_{\text{sh}}}{\partial \underline{\underline{C}}} \right) \quad (6)$$

The material parameters used for the stitches and yarns are shown in Table 1:

Table 1. Parameters of the constitutive model for yarn and stitch

| Symbol             | Physical interpretation                    | Value                    |
|--------------------|--|--------------------------|
| $K_{\text{elong}}$ | Tensile stiffness of fiber yarn            | 108500N                  |
| $K_{\text{comp}}$  | Compaction stiffness of fiber yarn         | 1.25MPa                  |
| $p$                | Compaction exponent                        | 1.84                     |
| $K_{\text{dist}}$  | Transverse shear stiffness of fiber yarn   | 0.6MPa                   |
| $K_{\text{sh}}$    | Longitudinal shear stiffness of fiber yarn | 2.2MPa                   |
| $E_s$              | Tensile stiffness of stitch                | 350MPa                   |
| $G_s$              | Bending stiffness of stitch                | 0.00056N mm <sup>2</sup> |

### Experiments on hemispherical forming

The hemispherical forming experiments are completed in LaMCoS laboratory. The experimental platform is shown in Fig. 4a. It mainly consists of the motion control system, camera, mirror, punch, blank holder, and die. The blank holder and die are made transparent to observe the material deformation during the draping process. The diameter of the punch is 150 mm and of the hole in the blank holder and die is 160 mm. Two cameras are used: one is positioned above the machine, capturing half of the sample (fixed with the machine bar, which does not move); the other camera is placed at a distance from the machine and in a horizontal orientation, allowing it to capture photos of the lower surface of the specimen using a mirror arranged at a 45° angle under the transparent tooling. The Zwick 100KN traction machine controls the punch displacement (75 mm), with a motion speed 25 mm · min<sup>-1</sup>.

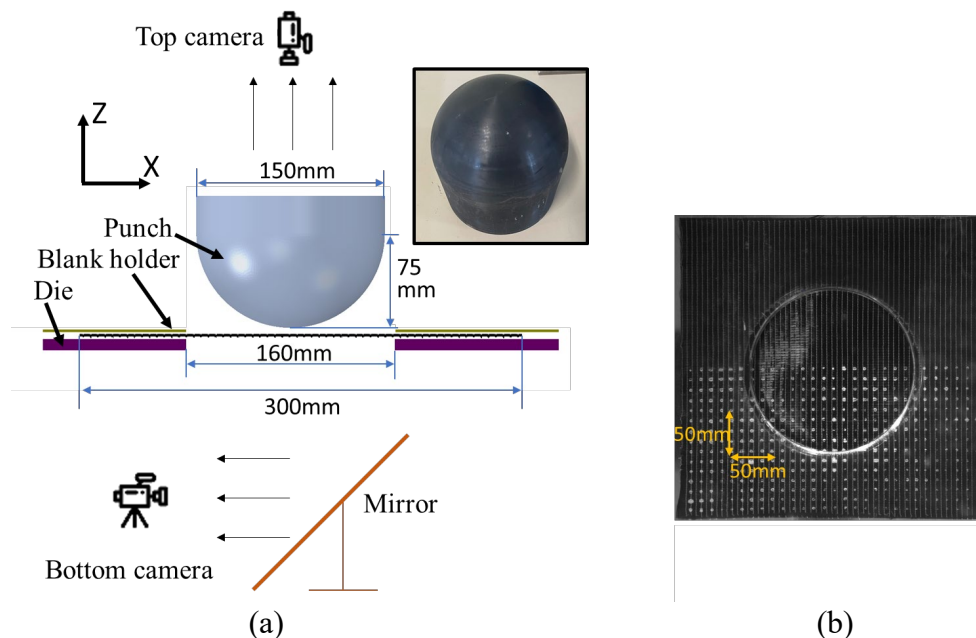


Fig. 4. Hemispherical forming experiments (a) Schema of Forming experimental platform (b) White marker painting

The sample used consists of one layer of biaxial NCF with dimensions of 300 mm by 300 mm, corresponding to a thickness of 0.8 mm. The specimen is initially in a square shape and placed on the die. The fiber yarn is oriented parallel to the edge of the square die. Three experimental forming

tests were carried out, two with white marker points and one without white marker points. White marker points are drawn on the bottom layers, as shown in Fig. 4b. They are in equal interval at 10 mm, and are 10 mm away from the sample boundary. This marker-based tracking approach is used to get the material deformation in different positions and calculate the shear angle when the material is deformed.

### Simulation on hemispherical forming

The forming tests are numerically simulated using ABAQUS/Explicit. Due to the symmetry of the hemispherical punch, the biaxial NCF are modeled using a quarter-sized sample to minimize computation costs. The quarter-sized model consists of 57,840 solid elements for warp and weft fiber yarns and 58,441 beam elements for stitches. The model for the punch, die and blank holder have the same dimensions as those used in the experimental tests. In the forming tests, these tools experience minimal deformations; therefore, they are modeled as rigid bodies (ABAQUS R3D4 elements). General friction law in ABAQUS is used for all the contact surfaces with coefficient 0.2. The die and blank holder are fixed in their positions throughout the simulation, while a draping displacement is prescribed for the punch. Coulomb friction contact is employed for the interaction between the tools and the fabric. The draping displacement is also set as 75 mm. The simulation is launched on the cluster with 20 CPU cores. The computation takes 6 days. Fig. 5a and b show the final deformed shape of biaxial NCF hemispherical forming simulation.

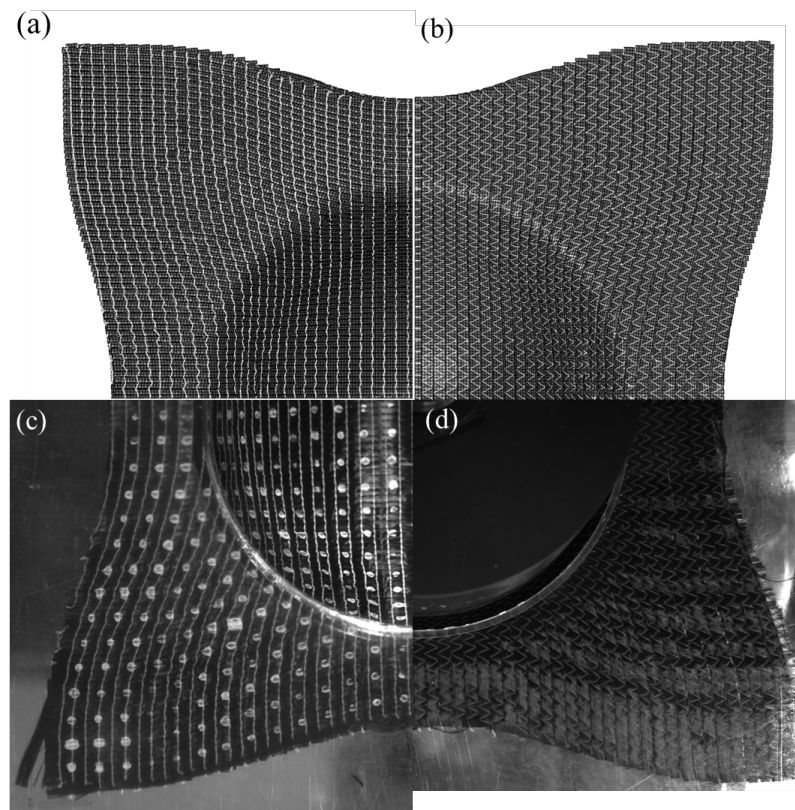


*Fig. 5. Draping of biaxial NCF on hemispherical shape. Simulation results of (a) weft fiber yarn view and (b) warp fiber yarn view; Experimental results of (c) weft fiber yarn view and (d) warp fiber yarn view.*

A comparison of the deformations reveals that the simulation produces an edge shape of the reinforcement resembling the one obtained experimentally. The outer contour of the simulation results can be drawn through the image processing on this 2D view and it can be observed that the simulation exhibits a similar material draw-in as the experimental result, as shown in Fig. 6.

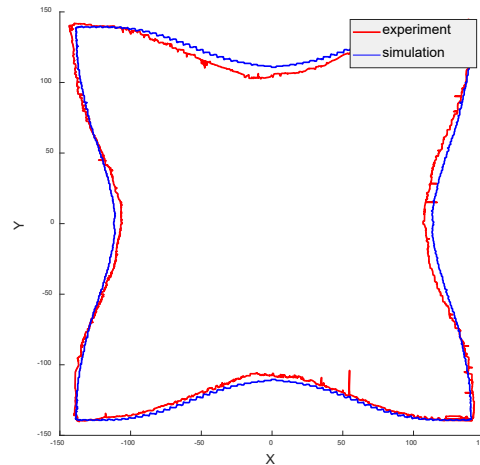


*Fig. 6. Comparison of material drawn-in between experiments (red line) and simulation (blue line)*

Another requirement for the simulation is its ability to accurately trace the yarn direction in the final composite part. The advantage of the mesoscopic model is that the two fiber orientations can be directly visualized and extracted from the numerical results. These directions are then employed to calculate the shear angles, which are subsequently compared with the experimental results. Since the structural integrity of biaxial NCF is enhanced through two fiber orientations and is further secured by stitches, only minimal gapping is noticeable on a smooth hemisphere shape and no gapping is observed in the simulation results.

## Conclusion

This study explores experimental forming tests on biaxial NCF utilizing a hemispherical punch shape. Subsequently, numerical simulations of the forming process are conducted employing a mesoscopic finite element model for biaxial NCF. The comparison of deformed shapes, material draw-in, and local shear angles between experimental and numerical results serves to validate the model's accuracy. No gapping defects are detected since hemispherical shape is a rather simple double-curved geometry with a smooth curvature. Further investigations into challenging shapes, such as the square box or tetrahedron, using the mesoscopic simulation approach can shed light on the occurrence of gapping defects.

## References

- [1] S. Lomov, 4 - understanding and modelling the effect of stitching on the geometry of non-crimp fabrics, in: S. V. Lomov (Eds.), *Non-Crimp Fabric Composites*, Woodhead Publishing Series in Composites Science and Engineering, Woodhead Publishing, 2011, pp. 84–102. <https://doi.org/10.1533/9780857092533.1.84>
- [2] S. Advani, E. Sozer, L. Mishnaevsky Jr, Pcess modeling in composite manufacturing, *plied Mechanics Reviews*. 56 (2003) B69-B70. <https://doi.org/10.1115/1.1584418>
- [3] S. Sihm, R. Y. Kim, K. Kawabe, S. W. Tsai, Eerimental studies of thin-ply laminated composites, *Composites Science and Technology*. 67 (2007) 996-1008. <https://doi.org/10.1016/j.compscitech.2006.06.008>
- [4] A. Schnabel, T. Gries, Production of non-crimp fabrics for composites, in: Stepan V. Lomov (Eds.), *Non-Crimp Fabric Composites*, Woodhead Publishing, 2011, pp. 3-41. <https://doi.org/10.1533/9780857092533.1.3>

- [5] M. Ashir, L. Hahn, A. Kluge, A. Nocke, C. Cherif, Development of innovative adaptive 3d fiber reinforced plastics based on shape memory alloys, *Composites Science and Technol.* 126 (2016) 43-51. <https://doi.org/10.1016/j.compscitech.2016.02.009>
- [6] P. Boisse, N. Hamila, E. Vidal-Sallé, F. Dumont, Simulation of wrinkling during textile composite reinforcement forming. Influence of tensile, in-plane shear and bending stiffnesses. *Composites Science and Technology*, 2011, 71 (5), pp.683. <https://doi.org/10.1016/j.compscitech.2011.01.011>
- [7] P. Boisse, B. Zouari, A. Gasser, A mesoscopic approach for the simulation of woven fibre composite forming, *Composites Science and Technol.* 65 (2005) 429-436. <https://doi.org/10.1016/j.compscitech.2004.09.024>
- [8] H. Kong and A.P. Mouritz and R. Paton, Tensile extension properties and deformation mechanisms of multiaxial non-crimp fabrics, *Composite Structures*. 66 (2004) 249-259. <https://doi.org/10.1016/j.compstruct.2004.04.046>
- [9] B. Schäfer, R. Zheng, P. Boisse, L. Kärger, Investigation of the compaction behavior of uni- and bidirectional non-crimp fabrics, *Materials Research Proceedings* 28 (2023) 331–338. <https://doi.org/10.21741/9781644902479-36>
- [10] F.J. Schirmaier and K.A. Weidenmann and L. Kärger and F. Henning, Characterisation of the draping behaviour of unidirectional non-crimp fabrics (UD-NCF). *Composites Part A: Applied Science and Manufacturing*. 80 (2016) 28-38. <https://doi.org/10.1016/j.compositesa.2015.10.004>
- [11] L. Kärger, S. Galkin, E. Kunze, M. Gude, B. Schäfer, Prediction of forming effects in UD-NCF by macroscopic forming simulation – Capabilities and limitations. *Proceedings of the 24th international conference on material forming*. (2021). <https://doi.org/10.25518/esaform21.355>
- [12] S. Bel and N. Hamila and P. Boisse and F. Dumont, Finite element model for NCF composite reinforcement preforming: Importance of inter-ply sliding, *Composites Part A: Applied Science and Manufacturing*. 43 (2012) 2269-2277. <https://doi.org/10.1016/j.compositesa.2012.08.005>
- [13] J. Schirmaier, D. Dörr, F. Henning, and L. Kärger, A macroscopic approach to simulate the forming behaviour of stitched unidirectional non-crimp fabrics (UD-NCF), *Composites: Part A* 102 (2017) 322–335. <http://dx.doi.org/10.1016/j.compositesa.2017.08.009>
- [14] S. Galkin, E. Kunze, L. Kärger, R. Böhm, M. Gude, Experimental and Numerical Determination of the Local Fiber Volume Content of Unidirectional Non-Crimp Fabrics with Forming Effects, *J. Compos. Sci.* 2019, 3(1), 19. <https://doi.org/10.3390/jcs3010019>
- [15] L. Li, Y. Zhao, H. Vuong, Y. Chen, J. Yang, Y. Duan, In-plane shear investigation of biaxial carbon non-crimp fabrics with experimental tests and finite element modeling, *Materials & Design*. 63 (2014) 757-765. <https://doi.org/10.1016/j.matdes.2014.07.007>
- [16] G. Creech, A. K. Pickett, Meso-modelling of Non-Crimp Fabric composites for coupled drape and failure analysis. *Journal of Materials Science*. 41 (2006) 6725–6736. <https://doi.org/10.1007/s10853-006-0213-6>
- [17] R. Zheng, B. Schäfer, A. Platzer, J. Colmars, N. Naouar, P. Boisse, A unit-cell mesoscale modelling of biaxial non-crimp-fabric based on a hyperelastic approach, *Materials Research Proceedings* 28 (2023) 285–292. <https://doi.org/10.21741/9781644902479-3.1>
- [18] S.V. Lomov, G. Huysmans, Y. Luo, R.S. Parnas, A. Prodromou, I. Verpoest, F.R. Phelan, Textile composites: modelling strategies, *Composites Part A: Applied Science and Manufacturing*. 32 (2001) 1379-1394. [https://doi.org/10.1016/S1359-835X\(01\)00038-0](https://doi.org/10.1016/S1359-835X(01)00038-0)

- [19] W. Wu, W. Li, Parametric modeling based on the real geometry of glass fiber unidirectional non-crimp fabric, *Textile Research Journal*. 89(2019). <https://doi.org/10.1177/0040517518824846>
- [20] P. Boisse, J. Colmars, N. Hamila, N. Naouar, Q. Steer, Bending and wrinkling of composite fiber preforms and prepregs. a review and new developments in the draping simulations, *Composites Part B: Engineering*. 141 (2018) 234–249. <https://doi.org/10.1016/j.compositesb.2017.12.061>
- [21] M. Ghazimoradi, E. A. Trejo, C. Butcher, J. Montesano, Characterizing the macroscopic response and local deformation mechanisms of a uni-directional non-crimp fabric, *Composites Part A: Applied Science and Manufacturing*. 156 (2022) 106857. <https://doi.org/10.1016/j.compositesa.2022.106857>
- [22] F. F. T. Peirce B.Sc., F.Inst.P., 26—the “handle” of cloth as a measurable quantity, *Journal of the Textile Institute Transactions*. 21 (1930) T377–T416. <https://doi.org/10.1080/19447023008661529>
- [23] A. Charmetant, E. Vidal-Sallé, P. Boisse, Hyperelastic modelling for mesoscopic analyses of composite reinforcements, *Composites Science and Technology* 71 (2011) 1623–1631. <https://doi.org/10.1016/j.compscitech.2011.07.004>
- [24] A. Iwata, T. Inoue, N. Naouar, P. Boisse, S. V. Lomov, Coupled meso-macro simulation of woven fabric local deformation during draping, *Compos. Part A* 118 (2019) 267-280. <https://doi.org/10.1016/j.compositesa.2019.01.004>